cdon and *boc* affect trunk neural crest cell migration through a non-cell autonomous reduction of hedgehog signaling in zebrafish slow-twitch muscle

Ezra Lencer PhD[1,2]

Rytis Prekeris PhD[2,3]

Kristin Artinger PhD[1,3]

1. Department of Craniofacial Biology, University of Colorado, United States

2. Department of Cell and Developmental Biology, University of Colorado, United States

3. Co-corresponding authors

Abstract

The immunoglobin superfamily members *cdon* and *boc* are transmembrane proteins implicated in regulating hedgehog signaling during vertebrate development. Recent work showing roles for these genes in axon guidance and neural crest cell migration further suggest that *cdon*/*boc* may play additional functions in regulating directed cell movements during development. Here we use novel and existing mutants to investigate a role for *cdon* and *boc* in zebrafish neural crest cell migration. We find that single *cdon* or *boc* mutant embryos exhibit normal neural crest phenotypes, but that neural crest migration is strikingly disrupted in double *cdon*/*boc* mutant embryos. We further show that this neural crest migration phenotype is associated with defects to the differentiation of slow-twitch muscle cells, and that this slow-twitch muscle phenotype is a consequence of reduced hedgehog signaling in mutant fish. While neural crest migratory ability is not affected in double mutant embryos, neural crest directionality is severely affected. These data suggest that neural crest migration defects are likely to be secondary to defects in slow-twitch muscle differentiation. Combined, our data add to a growing literature showing that *cdon* and *boc* act synergistically to promote hedgehog signaling during vertebrate development, and provide a foundation for using zebrafish to further study the function of these hedgehog receptor paralogs.

Introduction

During vertebrate development, neural crest cells (NCCs) migrate ventrally from the dorsal neural tube along conserved pathways in the embryo to contribute to numerous traits

37 such as the craniofacial skeleton, peripheral nervous system, and pigment (Theveneau and
38 Mayor, 2012). Defects in NCC migration result in multiple human hereditary disorders (Tobin et
39 al., 2008; Vega-Lopez et al., 2018), and modifications to NCC migration is associated with the
40 evolution of morphological diversity among some vertebrate taxa (Powder et al., 2014).
41 Further, diseases, such as metastatic melanoma, have been shown to progress through a
42 reactivation of a NCC-like migratory genetic program (Diener and Sommer, 2021; Kaufman et
43 al., 2016). Thus understanding the genetic regulation of NCC migration is fundamental to
44 understanding the etiology to multiple human diseases as well as a major development event
45 that occurs in every vertebrate embryo.
46 Current thinking stresses interactions among multiple mechanisms that when combined
47 coordinate NCC migration along highly conserved routes in the embryo (Mayor and Etienne-
48 Manneville, 2016). These include NCC intrinsic factors, such as genes regulating cell adhesion
49 and actin cytoskeleton (Clay and Halloran, 2011, 2013, 2014; Williams et al., 2018), as well as
50 cell extrinsic factors that affect the extracellular matrix (Perris and Perissinott, 2000; Szabo et
51 al., 2016), tissue stiffness (Shellard and Mayor, 2021), and chemical gradients (Barriga et al.,
52 2013; Olesnicky Killian et al., 2009; Shellard et al., 2018), which attract and funnel NCCs along
53 conserved paths in the embryo. Mediating cell intrinsic and extrinsic regulation of NCC
54 migration are cell-cell signaling interactions (Carmona-Fontaine et al., 2008; Mayor and
55 Etienne-Manneville, 2016; Scarpa et al., 2015; Szabo et al., 2016; Theveneau and Mayor, 2012).
56 These include the chemical gradients that attract and inhibit migrating NCCs, as well as the cell-
57 cell adhesion molecules that adhere NCCs to each other and mediate many cell-cell interactions

58 (Carmona-Fontaine et al., 2008; Mayor and Etienne-Manneville, 2016; Scarpa et al., 2015;
59 Szabo et al., 2016; Theveneau and Mayor, 2012; Vega-Lopez et al., 2017).
60 Recent work has implicated a role for the immunoglobin superfamily member protein
61 *cell adhesion associated, oncogene regulated* (*cdon*) as a cell surface protein regulating trunk
62 NCC (tNCC) migration in zebrafish (Powell et al., 2015). Morpholino knockdown of *cdon* results
63 in failed (tNCC) migration, with tNCCs mislocalizing N-cadherin and arresting migration at the
64 body midline. *cdon* and its paralog *BOC, brother of cell adhesion associated, oncogene*
65 *regulated* (*boc*), are vertebrate members of a larger gene family with identifiable orthologs in
66 other metazoan taxa that includes the drosophila paralogs *ihog* and *boi*. Recent work on both
67 vertebrate *cdon*/*boc* and *Drosophila ihog*/*boi* has established a role for these transmembrane
68 proteins in activating hedgehog signaling. *cdon* and *boc* act as co-receptors binding to hedgehog
69 ligand and patched receptor in order to promote smoothened signaling within cells. Other work
70 suggests that *cdon*/*boc* may commonly interact with additional signaling pathways including
71 Wnt signaling and Nodal signaling (Hong et al., 2020; Jeong et al., 2017). Further, *cdon* has been
72 shown to form a complex with N-cadherin/Cdc42/Bnip-2 in a hedgehog independent manner to
73 regulate actin cytoskeletal dynamics during myogenic differentiation in cell culture (Kang et al.,
74 2008; Lu and Krauss, 2010). *boc* has been shown to play a role in axon guidance, where it
75 operates as a receptor for hedgehog ligand to regulate proper neuronal growth (Connor et al.,
76 2005; Okada et al., 2006). Both *cdon*/*boc* and *ihog*/*boi* are often localized to the ends of long
77 membrane extensions (e.g. cytonemes in *Drosophila*), suggesting that these receptors may help
78 cells sense the wider external environment and communicate over long distances (Bilioni et al.,
79 2013; Ferent et al., 2019; Hall et al., 2021). It is thus possible that these transmembrane

80 proteins are reiteratively used as cell surface proteins to integrate multiple signals during
81 processes such as cell migration and axon guidance. While a role for *cdon* in tNCC migration has
82 been suggested (Powell et al., 2015), the function of *cdon*/*boc* in regulating NCC movements is
83 not fully understood.

84 In zebrafish, hedgehog signaling is currently thought to affect tNCC migration in a non-
85 cell autonomous manner by regulating the differentiation of adaxial cell mesoderm (Honjo and
86 Eisen, 2005). Adaxial cells form at the border of the notochord during the end of gastrulation
87 and differentiate into slow-twitch muscle cells that migrate laterally through the somatic
88 mesoderm (Elworthy et al., 2008; Wolff et al., 2003). A non-migratory population of adaxial cell
89 derivatives, called muscle pioneers, remain at the body midline. In hedgehog mutant embryos,
90 adaxial cells fail to differentiate into slow-twitch muscle/muscle pioneer derivatives (Elworthy
91 et al., 2008; Roy et al., 2001; Yin et al., 2018). Through a mechanism not fully understood, but
92 likely to depend on extracellular matrix deposition/modification (Banerjee et al., 2011;
93 Banerjee et al., 2013; Guillon et al., 2016; Honjo and Eisen, 2005), this slow-twitch muscle
94 differentiation is critical for normal NCC migration. Whether *cdon*/*boc* affect slow-twitch
95 muscle differentiation, however, is unknown (Bergeron et al., 2011), and it is further possible
96 that *cdon*/*boc* affect NCC development through NCC autonomous in addition to non-cell
97 autonomous mechanisms.

98 Here we use novel CRISPR/Cas9 generated mutations and existing mutants to
99 investigate the role of *cdon* and *boc* in tNCC migration and slow-twitch muscle differentiation.
100 We show that *cdon* and *boc* are expressed by tNCCs at low levels and by the adaxial mesoderm
101 at moderate levels. Loss of either *cdon* or *boc* individually has no observable effect on tNCC

102 migration nor slow-twitch muscle differentiation. However, embryos that are double mutant
103 for both *cdon* and *boc* exhibit both tNCC migratory defects as well as loss of slow-twitch muscle
104 mesoderm. We show that tNCC mobility is not impaired by loss of *cdon*/*boc* suggesting that the
105 tNCC migration defect is a non-cell autonomous consequence of slow-twitch muscle
106 differentiation. We further provide data suggesting that *cdon*/*boc* are modifying hedgehog
107 signal reception during mesoderm differentiation. Combined, our data contribute to a growing
108 literature showing that *cdon*/*boc* play a critical role in modulating hedgehog signaling across
109 multiple tissues during embryogenesis.
110

111 # Results

112 ***cdon/boc paralogs exhibit shared sequence conservation in extracellular functional domains***

113 The transmembrane robo-related proteins, *cdon* and *boc*, share a similar genomic
114 domain architecture that includes 4 immunoglobin (IG) domains, 3 fibronectin type 3 repeat
115 (FNIII) domains, and a cytosolic C-terminal tail (Figure 1A). A fifth IG domain is variable present
116 in *cdon* orthologs of tetrapod taxa (grey in Figure 1A). The FNIII domains have been implicated
117 in binding to hedgehog ligand and patched receptor (Izzi et al., 2011; Song et al., 2015), and
118 some evidence suggests that the c-terminal region is needed for protein localization in the cell
119 (Okumura et al., 2021).

120 As functional conservation is likely to be reflected by sequence conservation across
121 evolutionary time, we investigated the molecular evolution of *cdon*/*boc* orthologs across
122 vertebrate taxa. An alignment of *cdon* and *boc* amino acid sequences from 11 select jawed
123 vertebrate taxa shows that extracellular domains exhibit high conservation across taxa and

124 paralogs, suggesting that these extracellular domains are critical for gene function (Figure 1A).
125 In contrast, the C-terminal cytosolic tail exhibits relatively low sequence conservation (Kang et
126 al., 2002) suggesting that cytosolic region is evolutionarily labile to different selection
127 pressures.

128 Identifiable orthologs to *cdon* and *boc* are present in non-vertebrate bilaterian taxa.
129 These include *Drosophila* paralogs *ihog* and *boi*, whose function in hedgehog signaling has been
130 well characterized (Bilioni et al., 2013; Camp et al., 2010; Yao et al., 2006). However, the
131 orthology relationships between *cdon*/*boc* and non-vertebrate orthologs such as *ihog* and *boi*
132 are less well known. To explore the molecular evolution of this gene family we built a maximum
133 likelihood tree (phyml) using 44 amino acid sequences from taxa representative for major
134 bilaterian clades (Figure 1B). These data identify *cdon*/*boc* as shared vertebrate specific
135 paralogs that emerge from a duplication event at either the base of the vertebrate phylogeny
136 or along the gnathostome lineage following splitting from cyclostomes (hagfish and lamprey).
137 Importantly, these data are consistent with a hypothesis that *cdon*/*boc* originated during one of
138 the two vertebrate specific genome duplications (Dehal and Boore, 2005). Our analyses further
139 suggest that an independent gene duplication event led to the origins of *boi* and *ihog* paralogs
140 in drosophilids (Kang et al., 2002). Thus the co-orthologs *cdon*/*boc* and *boi*/*ihog* represent two
141 independent duplication events (Figure 1B)(Allen et al., 2011; Izzi et al., 2011; Sanchez-Arrones
142 et al., 2012), a finding that is concordant with gene trees made publicly available by the
143 TreeFam consortium (Li et al., 2006; Ruan et al., 2008).
144

145 *Generation of cdon and boc null alleles*

146 To further study the function of *cdon* and *boc* during zebrafish development we turned
147 to existing and novel mutations that are predicted to disrupt gene function (Figure 1C). Two
148 previously published ENU generated *boc* alleles were used in this study to characterize the
149 function of *boc* during zebrafish tNCC development. The *boc*/uml allele (Bergeron et al., 2011)
150 results in a predicted early stop (hereafter boc^{uml}). The boc^{co25} allele (Kearns et al., 2021) results
151 in an non-synonymous isoleucine to serine substitution in the third FNIII domain (Figure 1C). As
152 boc^{uml} and boc^{co25} alleles do not complement each other (Kearns et al., 2021), we focus our
153 analyses on boc^{co25} and note that we see similar results with boc^{uml}.
154 We used CRISPR/Cas9 to generate 2 novel mutations in *cdon*. Both alleles result in
155 predicted early stops (Figure 1C). The $cdon^{co1019}$ allele is a 229bp deletion that results in a
156 predicted early stop leading to a truncated protein prior to conserved IG domains. The
157 $cdon^{co1023}$ allele is a 5bp deletion in the FNIII(2) domain that similarly results in a predicted early
158 stop and a truncated protein prior to the transmembrane domain. We focus on the $cdon^{co1019}$
159 allele and note that we see similar results with the $cdon^{co1023}$ allele.
160
161 ***<u>cdon and boc transcripts are expressed in tNCCs and slow-twitch muscle cells</u>***
162 We next used multiplexed hybrid chain reaction *in situ* hybridization (HCR) in order to
163 ask where *cdon* and *boc* transcripts are expressed, and whether transcripts are detectable in
164 tNCCs and slow-twitch muscle progenitors. Unlike traditional enzymatic methods for *in situ*
165 hybridization, HCR allows single molecule measurement of gene expression at cellular
166 resolution, which enables identifying cells and cell types that express transcripts at relatively
167 low levels (Kearns et al., 2021).

168 We found *cdon* and *boc* transcripts to be abundant in the dorsal central nervous system
169 (CNS) of 24hpf-48hpf zebrafish embryos (Figure 2A-D), consistent with similar data from prior
170 studies (Bergeron et al., 2011; Cardozo et al., 2014; Kearns et al., 2021). This pattern is
171 established early in development. At 2 somites, *cdon* is expressed in the presumptive
172 notochord, while both *cdon* and *boc* are both expressed along the border of the neural plate in
173 cells that we suspect contribute to the dorsal neural tube at 24hpf (Figure 2A). Importantly,
174 while *boc* transcripts in the neural tube form a broad dorsal-ventral gradient (Kearns et al.,
175 2021), *cdon* transcripts are restricted to the dorsal-most roofplate cells and the ventral most
176 floorplate cells of the neural tube by 24hpf. In this way, *cdon* creates a dorsal sub-domain of
177 *boc* expression in the neural tube (Figure 2D). Floorplate cells also express hedgehog ligand,
178 and thus unlike *boc*, *cdon* is expressed in both hedgehog ligand producing and non-producing
179 cells within the CNS. This neural tube expression at 24hpf is broadly similar to expression
180 patterns reported in mouse embryos (Izzi et al., 2011; Kang et al., 2002; Mulieri et al., 2002;
181 MULIERI et al., 2000; Tenzen et al., 2006) suggesting that *cdon*/*boc* function in the CNS is likely
182 to be conserved.
183 We next asked whether migrating tNCCs express *cdon* and *boc*. Using the
184 tg(*sox10*:mRFP) transgene, we FAC sorted NCCs from the dissected trunks of 24hpf zebrafish
185 embryos and performed bulk RNA sequencing. These data suggest that tNCCs do express *cdon*
186 and *boc* at low levels (Figure 2E). We then asked if this expression is observable by HCR. Using
187 the tg(*sox10*:mRFP) transgene to again label NCCs, we segmented out *cdon* and *boc* HCR puncta
188 that overlap the *sox10* transgene. These data identify *cdon*/*boc* transcripts expressed by NCCs

189 at 24hpf (Figure 2F&G). While these data indicate that *cdon* and *boc* are expressed by tNCCs,
190 we note that tNCCs are expressing *cdon*/*boc* at levels far lower than the surrounding tissues.
191 Of note is that mesoderm appears to express *cdon* and *boc* at relatively high levels
192 (Figure 2), and prior studies had suggested that *boc* is expressed by slow-twitch muscle
193 mesoderm at 24hpf (Bergeron et al., 2011). We thus, next sought to identify whether *cdon*/*boc*
194 transcripts are in fact expressed by the developing slow-twitch muscle/adaxial cell mesoderm.
195 To do this we used the tgBAC(*prdm1a*:eGFP) transgene to label adaxial cells and slow-twitch
196 muscle mesoderm (Elworthy et al., 2008). At the 2 somite stage, adaxial cells are labeled with
197 the *prdm1a*:eGFP transgene, but we did not observe significant expression of *cdon*/*boc* in these
198 adaxial cells (Figure 2H). Instead, *cdon* and *boc* transcripts were largely restricted to the
199 developing neural plate and notochord (see above). By the 10 somite stage, *cdon* and *boc*
200 transcripts were observed throughout the paraxial mesoderm. Using the tg(*prdm1a*:eGFP)
201 transgene to segment out HCR transcripts expressed by adaxial cells, we were able to confirm
202 that *cdon* and *boc* are expressed by slow-twitch muscle progenitor cells (Figure 2I-J). At 24hpf,
203 differentiating slow-twitch muscle cells continue to express both *cdon* and *boc* (Figure 2K-L).
204 These data are consistent with bulk RNA-seq data from FAC-sorted trunk tgBAC(prdm1a:egFP)
205 positive cells at 24hpf (Figure 2E).
206 Taken together, our analyses indicate that *cdon* and *boc* are broadly expressed by
207 mesodermal tissues that include adaxial cell derived slow-twitch muscle cells, as well as tNCCs
208 at low levels, in addition to the developing neural tube.
209

210 *Trunk neural crest migration and adaxial mesoderm development are affected in cdon/boc*
211 *double mutants*

212 We next asked whether *cdon* and *boc* mutations affect tNCC migration and slow-twitch
213 muscle development by using the tg(*sox10*:mRFP) line to label migrating tNCCs and
214 immunostaining of a slow-twitch muscle specific myosin (DSHB F59) to label adaxial mesoderm
215 derivatives in 24 hpf embryos.

216 In wildtype embryos, tNCCs collectively migrate in streams down the middle of each
217 body segment (Figure 3). We found that this tNCC migratory phenotype was largely normal in
218 both single *cdon* and *boc* mutant embryos (Figure 3D-E). These data from homozygous mutant
219 embryos are in contrast to those reported by morpholino knockdown of *cdon* where tNCC
220 migratory streams fail to form (Powell et al., 2015). However, in double cdon^{co1019};boc^{co25}
221 mutants, tNCCs did fail to form distinguishable streams, and tNCC migration arrested at the
222 ventral neural tube/body midline (Figure 3F), a phenotypes that is similar to that observed in
223 *cdon* morphant embryos (Powell et al., 2015).

224 Similar to tNCC migration, we found that slow-twitch muscle differentiation was largely
225 normal in *cdon* and *boc* (Bergeron et al., 2011) single mutants. Only in double mutants did we
226 observe defects in slow-muscle cell differentiation (Figure 3C-F). Loss of slow-twitch muscle cell
227 differentiation was not complete, however, and posterior body segments tended to exhibit
228 greater loss of slow-twitch muscle differentiation than anterior segments. In double mutant
229 embryos, cells that did express slow-twitch muscle specific myosin (F59) appeared dysmorphic
230 with loosely packed myosin bundles relative to wildtype embryos (e.g. compare myosin bundle
231 width and packing in Figure 3).

232 Thus defects in tNCC migration and slow-twitch muscle cell differentiation are only
233 observed in *cdon*/*boc* double mutants.
234
235 *cdon and boc affect hedgehog signal transduction in slow-twitch muscle cells*
236 Since *cdon* and *boc* have previously been implicated in hedgehog signaling (Allen et al.,
237 2011; Zhang et al., 2006), we hypothesized that defects in both tNCC migration and slow-twitch
238 muscle cell differentiation were due to loss of hedgehog signaling that is only apparent in the
239 double mutants. To test this, we measured hedgehog signal reception by using the transgenic,
240 tg(8xGliBS:mCherry-NLS-Odc1) reporter line (hereafter 8xGli:mCherry) that drives nuclear
241 localized mCherry under the control of 8 tandem Gli binding sites (Mich et al., 2014). The
242 mCherry fluorophore contains an Odc1 destabilization domain the facilitates proteasomal
243 degradation to promote rapid fluorophore turnover within expressing cells.
244 At 24hpf, we observed mCherry positive nuclei in ventral neural tube cells and in slow-
245 twitch muscle fiber nuclei (Figure 3G)(Kearns et al., 2021; Mich et al., 2014). We never observed
246 mCherry positive nuclei in tNCCs (data not shown). In *cdon*^{co1019} and *boc*^{co25} mutants, the
247 number and signal intensity of nuclei that are 8xGli:mCherry positive was lower as compared to
248 wildtype siblings (Figure 3G-J). This decrease in signal was true for both cells in the neural tube
249 and slow-twitch muscle cells. Importantly, 8xGli:mCherry signal intensity varied across
250 genotypes, with *boc*^{co25} mutants displaying lower 8xGli:mCherry signal than *cdon*^{co1019} mutants,
251 and double mutants exhibiting low to no signal than all other genotypes. These data suggest
252 that *cdon*^{co1019} and *boc*^{co25} mutations are decreasing hedgehog signal reception in slow-twitch
253 muscle cells, which is consistent with a hypothesis that perturbations to hedgehog signaling is

254 responsible for the slow-twitch muscle differentiation phenotype in *cdon* and *boc* mutant
255 embryos (Barresi et al., 2000; Devoto et al., 1996).
256 Interestingly, the 8xGli:mCherry transgene reported substantively lower hedgehog
257 signal reception in single *cdon*^{co1019} and *boc*^{co25} mutant embryos that exhibit normal slow-twitch
258 muscle differentiation. These data suggest that slow-twitch muscle development is robust to
259 moderate perturbations to hedgehog signal. If this hypothesis is correct, we reasoned that *cdon*
260 and *boc* mutants should sensitize embryos to further pharmacological manipulation of
261 smoothened signaling with cyclopamine. To test this, we in-crossed double heterozygous
262 cdon$^{co1019/+}$;boc$^{co25/+}$ parents and treated embryos with 20uM cyclopamine from 50% epiboly to
263 24hpf. We then quantified the number of slow-twitch muscle fibers at 24hpf as a readout for
264 hedgehog signaling.
265 While single *boc* and *cdon* mutants treated with ethanol as a controls had a similar
266 number of slow-twitch muscle fibers as their wildtype ethanol treated siblings, *cdon* and *boc*
267 mutants treated with 20uM cyclopamine had significantly fewer slow-twitch muscle fibers than
268 their similarly cyclopamine treated wildtype siblings (Figure 4). This pattern was even more
269 striking for the double mutant. While double mutants treated with ethanol have an average of
270 approximately 5-6 slow-twitch muscle fibers per segment, double mutants lost all slow-twitch
271 muscle fibers when treated with 20uM cyclopamine. Furthermore, we noted qualitative
272 changes to slow-twitch muscle morphology in cyclopamine treated *cdon* and *boc* embryos.
273 Mutants treated with 20uM cyclopamine often exhibited gaps or missing slow-twitch muscle
274 fibers in body segments, and slow-twitch muscle fibers often appeared to have loosely packed
275 myosin.

276 We interpret these results to indicate that *cdon* and *boc* are modifying hedgehog signal
277 reception by slow-twitch muscles, and that loss of *cdon* or *boc* sensitize embryos to further
278 perturbations of hedgehog signal.
279
280 *Trunk neural crest cells lose directionality but not migratory ability in cdon/boc mutants*
281 The arrested NCC migratory phenotype in the double mutants is striking and could result from
282 either a loss of NCC migratory ability or a loss of directionality. To investigate this further we
283 used the tg(*sox10*:mRFP) transgene to label migrating tNCCs and live imaged NCC migration
284 through the trunk of the zebrafish embryo beginning at 22hpf (Figure 5). Migrating tNCCs were
285 manually tracked in imageJ using the mTrackJ plugin (Meijering et al., 2012). As we only
286 observed a tNCC migratory defect in the medial migrating streams, we limited our tracking of
287 cells to NCCs migrating along the medial route. We found that tNCC mobility was not disrupted
288 in *cdon*, *boc*, or double mutants as compared to wildtype controls. Across all genotypes, tNCCs
289 were qualitatively migratory, and general measures of mobility (e.g. Max velocity etc.) in
290 mutants were similar to that observed in wildtype controls (Figure 5D-G). In contrast, we
291 observed a significant loss of directional NCC movement in double cdon^{co1019};boc^{co25} mutant
292 embryos. In double mutants, tNCCs migrate to the body midline and then often move along the
293 anterior-posterior axis (Figure 5A-C), which is in contrast to the directed ventral movement
294 typical of wildtype embryos. This is seen quantitatively as lower migratory directionality and an
295 increased proportion of movements in lateral directions (Figure 5B&H). Single *cdon* or *boc*
296 mutants did not display migratory phenotypes that were different from that of wildtype
297 controls. Taken together, we interpret these results to indicate that loss of *cdon* and *boc* affects

298 tNCC directionality and path-finding ability, but that *cdon* and *boc* are not required for tNCC
299 mobility.
300
301 *cdon and boc mutants exhibit hedgehog-like craniofacial phenotypes*
302 While our data suggest that *cdon* and *boc* affect tNCC migration, we did not observe any
303 defects in cranial NCC migration (data not shown). However we did observe severe defects to
304 cranial cartilage morphology in *boc* and double mutants that are suggestive of other hedgehog
305 mutants. Homozygous *cdon*^{co1019} and *cdon*^{co1023} mutants, however, do not display noticeable
306 phenotypes (Figure 6). Further, we recovered homozygous *cdon* mutant adults that are fully
307 viable. While these *cdon* alleles are apparently not deleterious to organismal viability, we note
308 that when in combination with *boc* mutations these *cdon* alleles produce severe phenotypes
309 (see below) supporting the prediction that these alleles disrupt normal *cdon* function based on
310 the introduction of early stop codons.
311 In contrast to mutations in *cdon*, homozygous mutant *boc* embryos display striking
312 craniofacial and curved body phenotypes that are characteristic of reduced hedgehog signaling
313 (Bergeron et al., 2011). In the developing head, homozygous *boc*^{co25} and *boc*^{uml} mutants display
314 neurocranial defects with fused trabecular cartilages (Figure 6A). Defects in the development of
315 the neurocranial cartilages are classic midline phenotypes associated with mutations in
316 hedgehog pathway genes (Bergeron et al., 2011; Eberhart et al., 2006; Wada et al., 2005).
317 Interestingly, while mutations in smoothened or hedgehog ligand lead to complete loss of the
318 anterior ethmoid plate and fusion of the posterior trabecular cartilages (Eberhart et al., 2006;
319 Swartz et al., 2012; Wada et al., 2005), loss of *boc* only results in a relatively mild fusion of the

320 trabecular cartilages. Further, *boc* mutants have shortened or absent symplectic cartilages and
321 a striking ventral oriented ceratohyal cartilage that attaches at an obtuse angle to the head
322 (Figure 6). In the smoothened mutant (Swartz et al., 2012) and Dispatched 1 mutant (Schwend
323 and Ahlgren, 2009) a rudimentary ceratohyal projects ventrally (Swartz et al., 2012), suggesting
324 this mis-orientation of the ceratohyal is a canonical hedgehog phenotype. However, unlike in
325 these other mutants where the ceratohyal is greatly hypomorphic and jaw joints are often
326 fused, in *boc* mutants the ceratohyal is correctly formed and joints appear normal. To ask if this
327 ceratohyal orientation defect was secondary to defects in soft tissue we stained craniofacial
328 muscles with phalloidin and used the tg(*sox10*:mRFP) transgene to label NCC derived cartilages
329 (Figure 6B). Craniofacial muscles appear normal, suggesting that the orientation of the
330 ceratohyal in the *boc* mutant is due to cartilage element patterning and growth and not a
331 secondary defect resulting from disrupted muscle differentiation and or attachment.
332 Double mutants homozygous for both *cdon*^{co1019} and *boc*^{co25} exhibit more extreme
333 phenotypes consistent with a hypothesis that functional disruption of both *boc* and *cdon* leads
334 to a more dramatic loss of hedgehog signal reception. In double mutants, the symplectic is
335 absent, all craniofacial elements are hypomorphic, and neurocranial defects are more severe.
336 Double mutants variably present mild to severe forms of cardiac edema and typically have
337 more curved bodies than that observed in the *boc* mutants alone. We note that despite having
338 more severe phenotypes, the ethmoid plate was present in all *cdon*/*boc* double mutant
339 embryos observed, a curious observation given that the ethmoid plate is often lost in other
340 hedgehog mutants. Studied *cdon* and *boc* mutations do not complement each other and
341 *cdon*^{co1019}/*cdon*^{co1023};*boc*^{uml}/*boc*^{co25} embryos present phenotypes similar to homozygous

342 *cdon*^{co1019};*boc*^{co25} mutant embryos (Figure 6E). Taken together these data indicate that
343 *cdon*/*boc* mutants display phenotypes similar to other characterized hedgehog mutants
344 supporting the hypothesis that *cdon* and *boc* are modifying hedgehog signaling in the
345 developing embryo head. That double *cdon*/*boc* mutants have more severe phenotypes and
346 supports a hypothesis that *cdon*/*boc* paralogs have synergistic function in promoting hedgehog
347 signal reception.
348

349 **Discussion**

350 Here we show that *cdon* and *boc* affect trunk NCC migration as well as differentiation of
351 slow-twitch muscle cells. Despite some prior data suggesting that *cdon* may act cell
352 autonomously to affect tNCC migration, we find that neither *cdon* nor *boc* mutations have a
353 noticeable effect on NCC mobility. Rather, only in double *cdon/boc* mutants do we observe a
354 noticeable NCC migratory defect that is associated with loss of slow-twitch muscle mesoderm.
355 Prior research has shown that slow-twitch muscle differentiation requires hedgehog signaling
356 (Elworthy et al., 2008), and our data show that this slow-twitch muscle phenotype is due to a
357 reduction in hedgehog signaling within *cdon*/*boc* double mutants. Taken together we interpret
358 our data to suggest that a tNCC migratory defect in *cdon*/*boc* double mutants is a consequence
359 of defects in mesodermal differentiation (Banerjee et al., 2011; Banerjee et al., 2013; Honjo and
360 Eisen, 2005).
361 Our data add to a growing literature showing that *cdon* and *boc* act synergistically
362 during zebrafish development to modify hedgehog signal reception and regulate the
363 development of multiple traits (Echevarria-Andino and Allen, 2020; Song et al., 2015; Zhang et

364 al., 2011). Interestingly we found that *cdon* mutations alone do not produce any noticeable
365 phenotypes in zebrafish, and we are able to recover adult homozygous mutant zebrafish. This is
366 contrast to mouse, where loss of CDON results in mild holoprocephaly (Allen et al., 2011; Allen
367 et al., 2007; Echevarria-Andino and Allen, 2020; Zhang et al., 2011). While it is possible that our
368 *cdon* mutations do not result in full loss of function, we find this possibility unlikely. Both *cdon*
369 mutations lead predicted early stops prior to the transmembrane domain, which is similar to
370 the *boc*^{uml} mutation that does lead to a severe loss of function phenotype. Further, our *cdon*
371 mutants do impact *cdon* function as double *cdon*/*boc* mutants exhibit extreme phenotypes
372 suggestive of loss of *cdon* function. As both mutations lead to an early stop prior to the
373 transmembrane domain, production of any truncated *cdon* protein in these mutants should
374 lead to an extracellular pool of *cdon* that would be more likely to result in a dominant negative
375 phenotype than in a mild hypomorphic allele. However, we cannot fully rule out the possibility
376 that a late start rescues *cdon* protein resulting in a hypomorphic but functional receptor.
377 Unfortunately antibodies do not reliably recognize zebrafish *cdon* protein, and thus future
378 research could investigate whether other alleles targeting the FNIII(3) domain might result in
379 more severe phenotypes.
380 An alternative possibility, however, is that *cdon* and *boc*, as modifiers of hedgehog
381 signal, interact with other hedgehog pathway members resulting in species (or fish/mouse line
382 specific) phenotypic responses to *cdon* mutations. Thus in zebrafish other hedgehog pathway
383 members may provide robustness against *cdon* mutations allowing generally normal
384 phenotypic development. This hypothesis is supported by our findings that *cdon* and *boc*
385 mutations both sensitize embryos to cyclopamine treatment. Thus presumably *cdon* mutations

386 also sensitize embryos to genetic perturbations such as loss of other hedgehog pathway
387 members (or modifications to their gene expression). Intriguingly, we observed that *cdon* gene
388 expression is often nested within *boc* expression suggesting that *cdon* and *boc* act together to
389 modify hedgehog morphogen gradients. Kearns et al. 2021 found that *patched-2* (*ptch2*)
390 expression in the dorsal neural tube is expanded in *boc*^{co25} mutant embryos, suggesting that
391 loss of *boc* alone leads to more dorsal hedgehog reception (e.g. *ptch2* is a readout for hedgehog
392 signaling). These data were interpreted to suggest that *boc* sequesters hedgehog ligand driving
393 hedgehog signal reception to ventral tissues. Expanding on this hypothesis, we note that *cdon*
394 transcripts are positioned even more distally in the neural tube from hedgehog ligand source
395 than are *boc* transcripts. Thus together *boc* and *cdon* gradients may act as strong sequestering
396 agents to limit hedgehog signal activation to proper tissues and inhibit ligand activity in dorsal
397 neural tube cells.

398 Intriguingly, we and others note that *cdon* and *boc* are lowly expressed in a broad range
399 of tissues including the mesoderm, NCCs among others. Further *cdon*, but not *boc*, transcripts
400 are also co-expressed in hedgehog ligand producing cells, and some studies have suggested
401 that *cdon* plays a role in presenting hedgehog ligand to responsive cells (Hall et al., 2021). Thus
402 it is likely that *cdon* and *boc* are playing different roles in different tissues, and that cellular
403 context may be critical for determining the biological function of these receptors.

404 Here we present an early investigation into the phenotypes of *cdon* and *boc* mutations
405 in zebrafish as a foundation to further study the interact roles of these two paralogs. Future
406 work dissecting how these genes operate in different cellular contexts will address the diverse
407 roles of these genes in hedgehog pathway function.

408

409 # Materials and Methods

410 *Fish stocks, husbandry, and generation of mutants*

411 Adult fish and embryos were maintained at the University of Colorado Anschutz Medical
412 school according to standard zebrafish rearing protocols and guidelines for the rearing and
413 maintenance of vertebrate animals. The boc^{co25} mutant was previously recovered from an ENU
414 screen (Kearns et al., 2021). The boc^{uml} mutant was acquired from the Zebrafish International
415 Resource Center (boc^{ty54z}) and was described by (Bergeron et al., 2011).

416 We used CRISPR/Cas9 to generate novel mutations in *cdon*. Two sets of guide RNAs
417 (sgRNA) were designed to target either the 2nd and 3rd exons of cdon
418 (ggcagUUgaggagcagagUa, UggUaggagccUgUgagagc, UgcUUcagaaUcgcUgagag) or to target the
419 11th exon (UcgccaUUgagaUUgUgggg, cUccacgcgaaaUgcagUga). DNA oligos were annealed to a
420 common backbone scaffold that contains a T7 RNA polymerase site, which was used to
421 generate sgRNAs used for injections (Williams et al., 2018). For each sgRNA set, our final CRISPR
422 injection solution consisted of sgRNAs diluted to 20ng/uL, 1ug Cas9 Protein (Invitrogen TrueCut
423 V2), and 5ug Rhodamine Dextran in a total volume of 10uL. Approximated 2-4nl were injected
424 into the cell of a 1cell stage embryo, and F0 injected embryos were reared to adulthood. We
425 recovered a single allele for each sgRNA set. These include the cdon^{co1019} allele, which is a
426 229bp deletion that spans the second to third exon of *cdon*, removes the intronic sequence
427 between these exons, and is predicted to result in an early stop. The cdon^{co1023} allele is a 5bp
428 deletion resulting in a predicted early stop in the 11th exon that codes for the second FNIII

429 domain. F0 injected embryos were outcrossed for a minimum of two generations to minimize
430 effects of off target cutting.
431 Zebrafish *boc* and *cdon* mutants were crossed in to existing transgenic reporter lines
432 including the tg(*sox10*(7.2kb):mRFP)^{vu234} that labels NCCs with cytosolic mRFP (Kucenas et al.,
433 2008), and the gli reporter tg(8xgli-Xla.Cryaa:NLS-d1mCherry) line that has 8 gli-binding sites
434 driving a destabilized nuclear localized mCherry (Mich et al., 2014). The tgPAC(*prdm1a*:EGFP)
435 line was used to label adaxial mesoderm for reference (Elworthy et al., 2008).
436
437 *cdon/boc molecular conservation and gene tree*
438 Amino acid coding sequences for select bilaterian taxa were downloaded from NCBI GenBank.
439 Orthologous sequences were searched directly or identified through BLAST searches and
440 manual curation. The final set of sequences was chosen to include taxonomic representatives
441 for major bilaterian taxa for which high confidence sequences are available. Effort was made to
442 identify two paralogs for each taxon. Amino acid sequences were aligned using MUSCLE
443 (v3.8.31) with default parameters (Edgar, 2004). Amino acid conservation (Figure 1A) was
444 calculated by pairwise comparisons of *cdon*/*boc* homologues from 11 taxa (human, mouse,
445 chicken, *Anolis*, frog, bichir, Gar, sheepshead minnow, medaka, catfish, zebrafish) and plotted in
446 R by smoothing conservation values across 20 amino acid windows. Substitution models were
447 selected using ProtTest3 by AIC (Darriba et al., 2011). A maximum likelihood gene tree was built
448 using phyml (v3.3) and a JTT+I+G+F model on the entire unfiltered alignment with 1000
449 bootstraps (Guindon and Gascuel, 2003). Nodes with less than 60% bootstrap support were

450 collapsed into polytomies. We recovered similar results from filtered alignments that removed
451 poorly aligned regions and regions with gaps.
452
453 *Immunohistochemistry, in situ hybridization, and stains*
454 Adaxial mesoderm derivatives were stained by fluorescent immuno-histochemistry against a
455 slow-twitch muscle specific myosin (anti-MYH1A, F59, DSHB) at a concentration of 1:20 as
456 previously described (Elworthy et al., 2008; Nguyen-Chi et al., 2012). Hybrid Chain Reaction
457 (HCR) *in situ* hybridizations were performed as previously described (Choi et al., 2018; Lencer et
458 al., 2021). Custom HCR probes for zebrafish *cdon* and *boc* were acquired from Molecular
459 Instruments and used at a concentration of 2pMol/500uL Hybridization Buffer. Phalloidin-488
460 and phalloidin-647 stains (Thermo Fisher) were used at a concentration of 1:1000 to label
461 muscle tissue.
462
463 *Live imaging and tracking of migrating cells*
464 For live-imaging and tracking, neural crest cells were labelled using the tg(*sox10*:mRFP) line.
465 Embryos were mounted in 0.4% low melt agarose and neural crest cells were imaged over the
466 yolk extension every 5 minutes from ~22hpf to ~30hp on an Andor spinning disk confocal
467 microscope at 28C. Neural crest cells were manually tracked along the xy axis from maximum
468 projection images using the ImageJ mTrackJ plugin (Meijering et al., 2012). Drift was accounted
469 for using the Correct_3D_Drift.py plugin as implemented in ImageJ (Parslow et al., 2014).
470 Quantitative analysis of track mobility was performed in R. A small number of short tracks with
471 fewer than 30 points (2.5hrs) were excluded. As we also noted that NCCs often stopped

472 migrating upon reaching a ventral position we further limited tracks to a maximum of 6 hours in
473 order to capture cell migration. Limiting all tracks to the same time (e.g. number of points)
474 produces similar results. Roseplots depict cell movements with a velocity greater than
475 0.3uM/min, which empirically determined as a cutoff for capturing cell movements while also
476 excluding noise from drift and changes in cell shape. Using different cutoffs produced similar
477 results. Linear models were built in R by including track length as a fixed effect, and embryo
478 identity and date of imaging as random effects, with the packages lme4 (Bates et al., 2015),
479 lmerTest (Kuznetsova et al., 2017), and emmeans. Images of tracks were produced in napari
480 (Sofroniew et al., 2019).
481
482 *Pharmacological manipulation*
483 For pharmacological manipulation, embryos were manually dechorionated and treated with
484 20uM cyclopamine in ethanol (5uL/mL) from 50% epiboly to 24 hpf. Embryos that appeared
485 developmentally delayed were excluded.
486
487 *Imaging, Statitiscal Analysis, and biological replication*
488 All imaging was performed on either a Leica Sp8 Confocal, Andor spinning disk confocal, or
489 Olympus BX compound microscope. Image analysis and presentation was performed in ImageJ
490 or napari. All statistical analyses were performed in R. Experiments were repeated at least 3
491 times and biological variation was accounted for either in models and through inclusion of
492 biological replicates.
493

494 ## Acknowledgements

495 We thank members of the Artinger and Prekeris laboratories for comments on this manuscript
496 and project. This work was in part supported by GM122768 (to RP) and a University of Colorado
497 RNA Biosciences Initiateive award to EL and KA. EL was supported by National Institutes of
498 Health Ruth L. Kirschstein National Research Service Awards (T32CA17468 and F32HD103406).
499 EL, RP, and KA conceived of the study and wrote the manuscript. EL performed research and
500 analyses.

501

502 ## Figure Legends

503 **Figure 1. *cdon* and *boc* are transmembrane receptors and share conserved domain structure.**
504 **(A)** *cdon*/*boc* proteins share a domain structure that includes 4-5 immunoglobin (IG) domains, 3
505 fibronectin (FNIII) domains, a transmembrane (TM) region, and a cytosolic C-terminal tail. A
506 fifth IG domain (*) in *cdon* is found in some tetrapod taxa and indicated in grey. Percent
507 conservation (20 amino acid sliding window) is shown for an alignment of *cdon* and *boc* amino
508 acid sequences from 11 tetrapod and ray-finned fish taxa. Note that the extracellular domains
509 exhibit high sequence conservation, while the cytosolic region is less conserved. **(B)** Maximum
510 likelihood tree (phyml) for curated *cdon* and *boc* amino acid sequences from multiple bilaterian
511 taxa. Note independent duplications for Ihog/Boi in drosophilids and *cdon*/*boc* in vertebrates.
512 Node support was calculated based on 1000 bootstraps, and nodes with less than 60%
513 bootstrap support were collapsed. **(C)** Schematic of *cdon* and *boc* mutant alleles that are
514 characterized in the current study. Three alleles result in a predicted early stop, while boc^{co25}

515 contains a single nucleotide substitution that results in a non-synonymous isoleucine to serine
516 substitution.
517
518 **Figure 2**. ***cdon* and *boc* are expressed by NCCs and adaxial mesoderm cells**. (A-C) HCR shows
519 *cdon* (magenta) and boc (green) expression in the developing neural tube of 2 somite **(A)**, 24
520 hpf **(B)**, and 48 hpf **(C)** embryos. Note *cdon/boc* expression at the border of the neural plate **(A)**,
521 and in the roofplate/dorsal neural tube cells at 24 and 48 hpf. Additionally, *cdon* is expressed in
522 the ventral floorplate cells of the neural tube and notochord **(B&C)**. Weak *cdon*/*boc* expression
523 is observed throughout the mesoderm. Panels B&C are 20uM sections at the level of the yolk
524 extension (YE) in the trunk. **(D)** Schematic summarizing expression of *cdon*/*boc* in the neural
525 tube from panels B&C. Gradient of hedgehog ligand produced by notochord and floorplate cells
526 is indicated at left in grey, while expression of *cdon*/*boc* are indicated by magenta and green
527 respectively. (E) Bulk RNA-seq from FAC-sorted trunk NCCs (blue) and slow-twitch muscle cells
528 (red) suggests that both tissues express *cdon*/*boc*. Left & middle panels are boxplots showing
529 *cdon*/*boc* expression levels in 2 replicate samples of both cell types. Right panel shows
530 histogram of gene expression levels for all samples for all genes in the dataset aligned with
531 boxplots in left two panels. The location of genes that are markers for NCCs (*sox10*) or slow-
532 twitch muscle (*prdm1a*, *smyhc1*) are indicated by arrows. **(F&G)** HCR shows expression of
533 *cdon*/*boc* in trunk NCCs. **(F)** whole mount lateral view of the trunk of a 24 hpf embryo showing
534 expression of *cdon* (magenta), *boc* (green), and NCCs (grey) labeled by the tg(*sox10*:mRFP)
535 transgene. HCR puncta that overlap the *sox10* transgene were segmented out to visualize NCC
536 expression of *cdon* (F') or *boc* (F''). Segmented *cdon*/*boc* expression (*) are shown in yellow. (G)

537 Image from a 20uM cross section at the level of the yolk extension in the trunk shows NCCs
538 expressing *cdon*/*boc* transcripts. *cdon*/*boc* HCR puncta overlapping the tg(*sox10*:mRFP)
539 transgene (*) are shown in panels G' and G''. **(H-L)** Slow-twitch muscle cells express *cdon* and
540 *boc*. The tg(*prdm1a*:eGFP) transgene labeles adaxial cells at 2 somites **(H)**, and derivative slow-
541 twitch muscle cells at later stages **(I-L)**. *cdon*/*boc* transcripts do not overlap the adaxial cells at 2
542 somites **(H)**, but do overlap the slow-twitch muscle cells at 10 somites **(I-J)** and 24 hpf **(K-L)**.
543 Panel I shows 3D rendered of cross section from whole mount imaged embryos. HCR puncta
544 overlapping the tg(*prdm1a*:eGFP) transgene are shown in yellow in panels I' and I'' to highlight
545 slow-twitch muscle expression of *cdon*/*boc*. Panel J shows 3D rendered lateral view with HCR
546 puncta overlapping the *prdm1a* transgene (yellow). **(K)** At 24hpf slow-twitch muscle cells (grey)
547 continue to express *cdon*/*boc* transcripts. Panels K' and K'' show overlapping puncta. **(L)** 20uM
548 cross section of the trunk of a 24hpf embryo shows *cdon*/*boc* puncta overlapping the
549 tg(*prdm1a*:eGFP) transgene.
550
551 **Figure 3. *cdon* and *boc* double mutants have NCC migration and slow-twitch muscle**
552 **differentiation phenotypes and a reduction in hedgehog signal reception. (A)** Schematic cross
553 sections show NCC (red) and adaxial mesoderm (green) migration from approximately 10
554 somites to 20 somites. Adaxial mesoderm cells are specified adjacent to the notochord (nc) and
555 migrate laterally to differentiate into slow-twitch muscle fibers. Concurrent with adaxial cell
556 migration, NCCs migrate ventrally from dorsal neural tube (NT). **(B)** Left Panel shows 3D
557 rendering of a 10uM cross section from the trunk of a 15 somite embryo shows medially
558 positioned adaxial mesoderm (green) and ventrally migrating NCCs (red). NCCs are labeled with

559 the tg(*sox10*:mRFP) transgene, and adaxial mesoderm are labeled with the tg(*prdm1a*:eGFP)
560 transgene. Right panels show a lateral view of a 3D rendering of the trunk of a 24hpf embryo
561 shows slow-twitch muscle mesoderm (green) and migrating NCCs (red). Note the streams of
562 migrating NCCs and laterally position slow-twitch muscle. **(C-F)** Maximum projection images
563 show NCC streams (tg(*sox10*:mRFP)) and immunostaining for slow-twitch muscle specific
564 myosin (F59) for 24hpf wildtype embryos. Note loss of both streams and slow-twitch muscle
565 fibers in the double mutant. All images taken over the yolk extension in the trunk. **(G-J)**
566 Maximum projection images the tg(8xGli:mCherry) transgene in 24hpf embryos. Images taken
567 over the yolk extension. Note mCherry positive nuclei in the slow-twitch muscle mesoderm
568 (yellow arrows) and ventral neural tube (yellow arrowheads). 8xGli:mCherry signal
569 progressively decreases in *cdon*/*boc* mutants reflecting lower hedgehog signal reception.
570
571 **Figure 4. *cdon* and *boc* sensitize zebrafish embryos to a reduction in hedgehog signal by**
572 **cyclopamine treatment**. **(A)** Representative images show slow-twitch muscle fiber morphology
573 in 24hpf embryos treated with either 20uM cyclopamine or an equivalent volume of ethanol as
574 a control. Note *cdon* and *boc* mutants exhibit more severe phenotypes than their wildtype
575 siblings when treated with cyclopamine as evidenced by gaps in segments (arrows). Also note
576 complete loss of slow-twitch muscles in the double mutant treated with cyclopamine. **(B)**
577 Quantification of average number of slow-twitch muscle fibers per segment shows that *cdon*
578 and *boc* mutations are sensitizing embryos to cylclopamine treatment. Note that the number of
579 slow-twitch muscle fibers in single *cdon* and *boc* mutants are similar to wildtype siblings when

580 treated with ethanol, but significantly lower when treated with 20uM cyclopamine. Significance

581 values are from Tukey pairwise post-hoc tests: <0.05 = ∗, <0.001 = ∗∗∗.

582

583 **Figure 5. NCC directionality, but not migratory ability, is disrupted in the *cdon*/*boc* double**

584 **mutants. (A)** Maximum projection images show migrating NCCs (tg(*sox10*:mRFP)) in the trunks

585 of representative wildtype, *cdon*, *boc*, and double mutant embryos. Migratory tracks from

586 individual cells are shown by colored lines. Note that NCCs form horizontal tracks at the body

587 midline in the double mutant. **(B)** Matched Roseplots (left panels) showing directional

588 movement and line plots (right panel) showing tracks for NCCs in each genotype. For both

589 panels, dorsal is up and anterior is to the left. Samples sizes reflect #tracks/#Embryos. Note that

590 ventral directionality of NCC movement is lower in the double mutant as best seen by the rose

591 plot. **(C)** NCC migration tracks (colored lines) are overlayed onto outlines of the body (grey

592 dashed lines) for representative embryos. Note the vertical aligned tracks in the wildtype, *cdon*,

593 and *boc* mutants that reflects ventral migration. Tracks form horizontal lines in the double

594 mutant reflecting NCC migratory movements along the anterior-posterior axis. Body outlines

595 were traced from the starting timepoint and do not reflect growth. Somite segments in the

596 double mutant are wider and dysmorphic. **(D-H)** Boxplots show quantification of NCC migration

597 for maximum velocity **(D)**, mean velocity **(E)**, track length **(F)**, track displacement **(G)**, and track

598 straightness **(H)**. Note that the double *cdon*/*boc* mutants are the only condidtion that is

599 significantly different from wildtype embryos in track straightness. Small grey points are

600 individual track values, large colored points are means for individuals, boxplots reflect

601 variability across tracks. **(I)** Schematic of track straightness which is calculated as track

602 displacement dived by track length.

603

604 **Figure 6. *cdon* and *boc* are important for proper craniofacial development. (A)** Representative

605 images of 7dpf larvae show craniofacial cartilages in *boc*^{co25}, *cdon*^{co1019}, and double mutants as

606 shown by alcian blue (cartilage, blue) and alizarin red (bone, red) stain. Note the medial

607 trabecular elements of the neurocranium are disrupted in *boc* and double mutants (arrows).

608 Also note a ventral projecting ceratohyal cartilage in the *boc* and double mutant (arrow head).

609 All phenotypes are more severe in the double mutant which also has hypomorphic craniofacial

610 cartilages and lacks the symplectic arm of the hyosymplectic cartilage. Scale bars are 20uM. ch

611 = ceratohyal, ep = ethmoid plate, hs = hyosymplectic, mc = Meckel's cartilage, op = opercle, pq

612 = palatoquadrate, pt = pterygoid process, sy = symplectic, tr = trabecula. **(B)** Representative

613 maximum projection images of 7dpf larvae stained with phalloidin (green) to label muscles.

614 Cartilages are labeled by the tg(*sox10*:mRFP) transgene that marks NCCs (magenta). Arrow

615 head points to ventral oriented ceratohyal in boc and double mutants. Note that craniofacial

616 muscles are normal across all genotypes suggesting that mis-orientation of the ceratohyal is

617 unlikely to be a secondary consequence of disruption to soft-tissue morphology. **(C)**

618 Quantification of ceratohyal angle shows that *boc*^{co25} and double mutants have significantly

619 more ventral projecting ceratohyals. **(D)** Quantification of symplectic length showing that the

620 length of the symplectic is shorter in *cdon*/*boc* mutants. Significance in panels B&C is Tukey

621 post-hoc test relative to wildtype values. Sample sizes are wildtype = 6, cdon = 8, boc = 11,

Double = 6. **(E)** A cdon^{co1019}/cdon^{co1023};boc^{co25}/boc^{uml} embryo showing that different *cdon* and *boc* alleles do not complement each other.

627 # References

628 Allen, B.L., Song, J.Y., Izzi, L., Althaus, I.W., Kang, J.S., Charron, F., Krauss, R.S., McMahon, A.P.,
629 2011. Overlapping roles and collective requirement for the coreceptors GAS1, CDO, and BOC in
630 SHH pathway function. Dev Cell 20, 775-787.

631 Allen, B.L., Tenzen, T., McMahon, A.P., 2007. The Hedgehog-binding proteins Gas1 and Cdo
632 cooperate to positively regulate Shh signaling during mouse development. Genes Dev 21, 1244-
633 1257.

634 Banerjee, S., Gordon, L., Donn, T.M., Berti, C., Moens, C.B., Burden, S.J., Granato, M., 2011. A
635 novel role for MuSK and non-canonical Wnt signaling during segmental neural crest cell
636 migration. Development 138, 3287-3296.

637 Banerjee, S., Isaacman-Beck, J., Schneider, V.A., Granato, M., 2013. A novel role for Lh3
638 dependent ECM modifications during neural crest cell migration in zebrafish. PLoS One 8,
639 e54609.

640 Barresi, M.J.F., Stickney, H.L., Devoto, S.H., 2000. The zebrafish slow-muscle-omitted gene
641 product is required fro Hedgehog signal transduction and the development of slow muscle
642 identity. Development 127, 2189-2199.

643 Barriga, E.H., Maxwell, P.H., Reyes, A.E., Mayor, R., 2013. The hypoxia factor Hif-1alpha controls
644 neural crest chemotaxis and epithelial to mesenchymal transition. J Cell Biol 201, 759-776.

645 Bates, D., Mächler, M., Bolker, B., Walker, S., 2015. Fitting Linear Mixed-Effects Models
646 Usinglme4. Journal of Statistical Software 67.

647 Bergeron, S.A., Tyurina, O.V., Miller, E., Bagas, A., Karlstrom, R.O., 2011. Brother of cdo
648 (umleitung) is cell-autonomously required for Hedgehog-mediated ventral CNS patterning in
649 the zebrafish. Development 138, 75-85.

650 Bilioni, A., Sanchez-Hernandez, D., Callejo, A., Gradilla, A.C., Ibanez, C., Mollica, E., Carmen
651 Rodriguez-Navas, M., Simon, E., Guerrero, I., 2013. Balancing Hedgehog, a retention and release
652 equilibrium given by Dally, Ihog, Boi and shifted/DmWif. Dev Biol 376, 198-212.

653 Camp, D., Currie, K., Labbé, A., Meyel, D.J.v., Charron, F.d.r., 2010. Ihog and Boi are essential for
654 Hedgehog signaling in Drosophila. Neural Development 5.

655 Cardozo, M.J., Sanchez-Arrones, L., Sandonis, A., Sanchez-Camacho, C., Gestri, G., Wilson, S.W.,
656 Guerrero, I., Bovolenta, P., 2014. Cdon acts as a Hedgehog decoy receptor during proximal-
657 distal patterning of the optic vesicle. Nat Commun 5, 4272.

658 Carmona-Fontaine, C., Matthews, H.K., Kuriyama, S., Moreno, M., Dunn, G.A., Parsons, M.,
659 Stern, C.D., Mayor, R., 2008. Contact inhibition of locomotion in vivo controls neural crest
660 directional migration. Nature 456, 957-961.

661 Choi, H.M.T., Schwarzkopf, M., Fornace, M.E., Acharya, A., Artavanis, G., Stegmaier, J., Cunha,
662 A., Pierce, N.A., 2018. Third-generation in situ hybridization chain reaction: multiplexed,
663 quantitative, sensitive, versatile, robust. Development 145.

664 Clay, M.R., Halloran, M.C., 2011. Regulation of cell adhesions and motility during initiation of
665 neural crest migration. Curr Opin Neurobiol 21, 17-22.

666 Clay, M.R., Halloran, M.C., 2013. Rho activation is apically restricted by Arhgap1 in neural crest
667 cells and drives epithelial-to-mesenchymal transition. Development 140, 3198-3209.

668 Clay, M.R., Halloran, M.C., 2014. Cadherin 6 promotes neural crest cell detachment via F-actin
669 regulation and influences active Rho distribution during epithelial-to-mesenchymal transition.
670 Development 141, 2506-2515.

671 Connor, R.M., Allen, C.L., Devine, C.A., Claxton, C., Key, B., 2005. BOC, brother of CDO, is a
672 dorsoventral axon-guidance molecule in the embryonic vertebrate brain. J Comp Neurol 485,
673 32-42.

674 Darriba, D., Taboada, G.L., Doallo, R., Posada, D., 2011. ProtTest 3: fast selection of best-fit
675 models of protein evolution. Bioinformatics 27, 1164-1165.

676 Dehal, P., Boore, J.L., 2005. Two rounds of whole genome duplication in the ancestral
677 vertebrate. PLoS Biol 3, e314.

678 Devoto, S.H., Melancon, E., Eisen, J.S., Westerfield, M., 1996. Identification of separate slow
679 and fast muscle precursor cells in vivo, prior to somite formation. Development 122, 3371-
680 3380.

681 Diener, J., Sommer, L., 2021. Reemergence of neural crest stem cell-like states in melanoma
682 during disease progression and treatment. Stem Cells Transl Med 10, 522-533.

683 Eberhart, J.K., Swartz, M.E., Crump, J.G., Kimmel, C.B., 2006. Early Hedgehog signaling from
684 neural to oral epithelium organizes anterior craniofacial development. Development 133, 1069-
685 1077.

686 Echevarria-Andino, M.L., Allen, B.L., 2020. The hedgehog co-receptor BOC differentially
687 regulates SHH signaling during craniofacial development. Development 147.

688 Edgar, R.C., 2004. MUSCLE: multiple sequence alignment with high accuracy and high
689 throughput. Nucleic Acids Res 32, 1792-1797.

690 Elworthy, S., Hargrave, M., Knight, R., Mebus, K., Ingham, P.W., 2008. Expression of multiple
691 slow myosin heavy chain genes reveals a diversity of zebrafish slow twitch muscle fibres with
692 differing requirements for Hedgehog and Prdm1 activity. Development 135, 2115-2126.

693 Ferent, J., Giguere, F., Jolicoeur, C., Morin, S., Michaud, J.F., Makihara, S., Yam, P.T., Cayouette,
694 M., Charron, F., 2019. Boc Acts via Numb as a Shh-Dependent Endocytic Platform for Ptch1
695 Internalization and Shh-Mediated Axon Guidance. Neuron 102, 1157-1171 e1155.

696 Guillon, E., Bretaud, S., Ruggiero, F., 2016. Slow Muscle Precursors Lay Down a Collagen XV
697 Matrix Fingerprint to Guide Motor Axon Navigation. J Neurosci 36, 2663-2676.

698 Guindon, S., Gascuel, O., 2003. A simple, fast, and accurate algorithm to estimate large
699 phylogenies by maximum likelihood. Syst Biol 52, 696-704.

700 Hall, E.T., Dillard, M.E., Stewart, D.P., Zhang, Y., Wagner, B., Levine, R.M., Pruett-Miller, S.M.,
701 Sykes, A., Temirov, J., Cheney, R.E., Mori, M., Robinson, C.G., Ogden, S.K., 2021. Cytoneme
702 delivery of Sonic Hedgehog from ligand-producing cells requires Myosin 10 and a Dispatched-
703 BOC/CDON co-receptor complex. Elife 10.

704 Hong, M., Christ, A., Christa, A., Willnow, T., Krauss, R.S., 2020. Cdon Mutation and Fetal
705 Alcohol Converge on Nodal Signaling in a Gene-Environment Interaction Model of
706 Holoprosencephaly. BioRxiv.

707 Honjo, Y., Eisen, J.S., 2005. Slow muscle regulates the pattern of trunk neural crest migration in
708 zebrafish. Development 132, 4461-4470.

709 Izzi, L., Levesque, M., Morin, S., Laniel, D., Wilkes, B.C., Mille, F., Krauss, R.S., McMahon, A.P.,
710 Allen, B.L., Charron, F., 2011. Boc and Gas1 each form distinct Shh receptor complexes with
711 Ptch1 and are required for Shh-mediated cell proliferation. Dev Cell 20, 788-801.

712 Jeong, M.H., Kim, H.J., Pyun, J.H., Choi, K.S., Lee, D.I., Solhjoo, S., O'Rourke, B., Tomaselli, G.F.,
713 Jeong, D.S., Cho, H., Kang, J.S., 2017. Cdon deficiency causes cardiac remodeling through
714 hyperactivation of WNT/beta-catenin signaling. Proc Natl Acad Sci U S A 114, E1345-E1354.

715 Kang, J.-S., Mulieri, P.J., Hu, Y., Taliana, L., Krauss, R.S., 2002. BOC, an Ig superfamily member,
716 associates with CDO to positively regulate myogenic differentiation. EMBO J 21, 114-124.

717 Kang, J.S., Bae, G.U., Yi, M.J., Yang, Y.J., Oh, J.E., Takaesu, G., Zhou, Y.T., Low, B.C., Krauss, R.S.,
718 2008. A Cdo-Bnip-2-Cdc42 signaling pathway regulates p38alpha/beta MAPK activity and
719 myogenic differentiation. J Cell Biol 182, 497-507.

720 Kaufman, C.K., Mosimann, C., Fan, Z.P., Yang, S., Thomas, A.J., Ablain, J., Tan, J.L., Fogley, R.D.,
721 van Rooijen, E., Hagedorn, E.J., Ciarlo, C., White, R.M., Matos, D.A., Puller, A.C., Santoriello, C.,
722 Liao, E.C., Young, R.A., Zon, L.I., 2016. A zebrafish melanoma model reveals emergence of
723 neural crest identity during melanoma initiation. Science 351, aad2197.

724 Kearns, C.A., Walker, M., Ravanelli, A.M., Scott, K., Arzbecker, M.R., Appel, B., 2021. Zebrafish
725 spinal cord oligodendrocyte formation requires boc function. BioRxiv.

726 Kucenas, S., Snell, H., Appel, B., 2008. nkx2.2a promotes specification and differentiation of a
727 myelinating subset of oligodendrocyte lineage cells in zebrafish. Neuron glia biology 4, 71-81.

728 Kuznetsova, A., Brockhoff, P.B., Christensen, R.H.B., 2017. lmerTest Package: Tests in Linear
729 Mixed Effects Models. Journal of Statistical Software 82, 1-26.

730 Lencer, E., Prekeris, R., Artinger, K.B., 2021. Single-cell RNA analysis identifies pre-migratory
731 neural crest cells expressing markers of differentiated derivatives. Elife 10.

732 Li, H., Coghlan, A., Ruan, J., Coin, L.J., Heriche, J.K., Osmotherly, L., Li, R., Liu, T., Zhang, Z.,
733 Bolund, L., Wong, G.K., Zheng, W., Dehal, P., Wang, J., Durbin, R., 2006. TreeFam: a curated
734 database of phylogenetic trees of animal gene families. Nucleic Acids Res 34, D572-580.

735 Lu, M., Krauss, R.S., 2010. N-cadherin ligation, but not Sonic hedgehog binding, initiates Cdo-
736 dependent p38alpha/beta MAPK signaling in skeletal myoblasts. Proc Natl Acad Sci U S A 107,
737 4212-4217.

738 Mayor, R., Etienne-Manneville, S., 2016. The front and rear of collective cell migration. Nat Rev
739 Mol Cell Biol 17, 97-109.

740 Meijering, E., D'zyubachyk, O., Smal, I., 2012. Methods for Cell and Particle Tracking. Methods
741 in Enzymology 504, 183-200.

742 Mich, J.K., Payumo, A.Y., Rack, P.G., Chen, J.K., 2014. In vivo imaging of Hedgehog pathway
743 activation with a nuclear fluorescent reporter. PLoS One 9, e103661.

744 Mulieri, P.J., Kang, J.S., Sassoon, D.A., Krauss, R.S., 2002. Expression of the boc gene during
745 murine embryogenesis. Dev Dyn 223, 379-388.

746 MULIERI, P.J., OKADA, A., SASSOON, D.A., MCCONNELL, S.K., KRAUSS, A.R.S., 2000.
747 Developmental Expression Pattern of the cdo Gene. Developmental Dynamics 219, 40-49.

748 Nguyen-Chi, M.E., Bryson-Richardson, R., Sonntag, C., Hall, T.E., Gibson, A., Sztal, T., Chua, W.,
749 Schilling, T.F., Currie, P.D., 2012. Morphogenesis and cell fate determination within the adaxial
750 cell equivalence group of the zebrafish myotome. PLoS Genet 8, e1003014.

751 Okada, A., Charron, F., Morin, S., Shin, D.S., Wong, K., Fabre, P.J., Tessier-Lavigne, M.,
752 McConnell, S.K., 2006. Boc is a receptor for sonic hedgehog in the guidance of commissural
753 axons. Nature 444, 369-373.

754 Okumura, F., Oki, N., Fujiki, Y., Ikuta, R., Osaki, K., Hamada, S., Nakatsukasa, K., Hisamoto, N.,
755 Hara, T., Kamura, T., 2021. ZSWIM8 is a myogenic protein that partly prevents C2C12
756 differentiation. Sci Rep 11, 20880.

757 Olesnicky Killian, E.C., Birkholz, D.A., Artinger, K.B., 2009. A role for chemokine signaling in
758 neural crest cell migration and craniofacial development. Dev Biol 333, 161-172.

759 Parslow, A., Cardona, A., Bryson-Richardson, R., 2014. Sample drift correctino following 3D
760 confocal time-lapse imaging. J. Vis. Exp. 12.

761 Perris, R., Perissinott, D., 2000. Role of the extracellular matrix during neural crest cell
762 migration. Mechanisms of Development 95, 3-21.

763 Powder, K.E., Cousin, H., McLinden, G.P., Craig Albertson, R., 2014. A nonsynonymous mutation
764 in the transcriptional regulator lbh is associated with cichlid craniofacial adaptation and neural
765 crest cell development. Mol Biol Evol 31, 3113-3124.

766 Powell, D.R., Williams, J.S., Hernandez-Lagunas, L., Salcedo, E., O'Brien, J.H., Artinger, K.B.,
767 2015. Cdon promotes neural crest migration by regulating N-cadherin localization. Dev Biol 407,
768 289-299.

769 Roy, S., Wolff, C., Ingham, P.W., 2001. The u-boot mutation identifies a Hedgehog-regulated
770 myogenic switch for fiber-type diversification in the zebrafish embryo. Genes Dev 15, 1563-
771 1576.

772 Ruan, J., Li, H., Chen, Z., Coghlan, A., Coin, L.J., Guo, Y., Heriche, J.K., Hu, Y., Kristiansen, K., Li, R.,
773 Liu, T., Moses, A., Qin, J., Vang, S., Vilella, A.J., Ureta-Vidal, A., Bolund, L., Wang, J., Durbin, R.,
774 2008. TreeFam: 2008 Update. Nucleic Acids Res 36, D735-740.

775 Sanchez-Arrones, L., Cardozo, M., Nieto-Lopez, F., Bovolenta, P., 2012. Cdon and Boc: Two
776 transmembrane proteins implicated in cell-cell communication. Int J Biochem Cell Biol 44, 698-
777 702.

778 Scarpa, E., Szabo, A., Bibonne, A., Theveneau, E., Parsons, M., Mayor, R., 2015. Cadherin Switch
779 during EMT in Neural Crest Cells Leads to Contact Inhibition of Locomotion via Repolarization of
780 Forces. Dev Cell 34, 421-434.

781 Schwend, T., Ahlgren, S.C., 2009. Zebrafish con/disp1 reveals multiple spatiotemporal
782 requirements for Hedgehog-signaling in craniofacial development. BMC Dev Biol 9, 59.

783 Shellard, A., Mayor, R., 2021. Collective durotaxis along a self-generated stiffness gradient in
784 vivo. Nature 600, 690-694.

785 Shellard, A., Szabo, A., Trepat, X., Mayor, R., 2018. Supracellular contraction at the rear of
786 neural crest cell groups drives collective chemotaxis. Science 362, 339-343.

787 Sofroniew, N., Lambert, T., Evans, K., Nunez-Iglesias, J., Bokota, G., Peña-Castellanos, G.,
788 Winston, P., Yamauchi, K., Bussonnier, M., Pop, D.D., Liu, Z., ACS, Pam, alisterburt, Buckley, G.,
789 Sweet, A., Gaifas, L., Rodríguez-Guerra, J., Migas, L., Hilsenstein, V., Bragantini, J., Lee, G.R.,
790 Hector, Freeman, J., Boone, P., Lowe, A.R., Gohlke, C., Royer, L., PIERRÉ, A., Har-Gil, H., 2019.
791 napari: a multi-dimensional image viewer for python.

792 Song, J.Y., Holtz, A.M., Pinskey, J.M., Allen, B.L., 2015. Distinct structural requirements for
793 CDON and BOC in the promotion of Hedgehog signaling. Dev Biol 402, 239-252.

794 Swartz, M.E., Nguyen, V., McCarthy, N.Q., Eberhart, J.K., 2012. Hh signaling regulates patterning
795 and morphogenesis of the pharyngeal arch-derived skeleton. Dev Biol 369, 65-75.

796 Szabo, A., Melchionda, M., Nastasi, G., Woods, M.L., Campo, S., Perris, R., Mayor, R., 2016. In
797 vivo confinement promotes collective migration of neural crest cells. J Cell Biol 213, 543-555.

798 Tenzen, T., Allen, B.L., Cole, F., Kang, J.S., Krauss, R.S., McMahon, A.P., 2006. The cell surface
799 membrane proteins Cdo and Boc are components and targets of the Hedgehog signaling
800 pathway and feedback network in mice. Dev Cell 10, 647-656.

801 Theveneau, E., Mayor, R., 2012. Neural crest delamination and migration: from epithelium-to-
802 mesenchyme transition to collective cell migration. Dev Biol 366, 34-54.

803 Tobin, J.L., Di Franco, M., Eichers, E., May-Simera, H., Garcia, M., Yan, J., Quinlan, R., Justice,
804 M.J., Hennekam, R.C., Briscoe, J., Tada, M., Mayor, R., Burns, A.J., Lupski, J.R., Hammond, P.,
805 Beales, P.L., 2008. Inhibition of neural crest migration underlies craniofacial dysmorphology and
806 Hirschsprung's disease in Bardet-Biedl syndrome. Proc Natl Acad Sci U S A 105, 6714-6719.

807 Vega-Lopez, G.A., Cerrizuela, S., Aybar, M.J., 2017. Trunk neural crest cells: formation, migration
808 and beyond. Int J Dev Biol 61, 5-15.

809 Vega-Lopez, G.A., Cerrizuela, S., Tribulo, C., Aybar, M.J., 2018. Neurocristopathies: New insights
810 150 years after the neural crest discovery. Dev Biol 444 Suppl 1, S110-S143.

811 Wada, N., Javidan, Y., Nelson, S., Carney, T.J., Kelsh, R.N., Schilling, T.F., 2005. Hedgehog
812 signaling is required for cranial neural crest morphogenesis and chondrogenesis at the midline
813 in the zebrafish skull. Development 132, 3977-3988.

814 Williams, J.S., Hsu, J.Y., Rossi, C.C., Artinger, K.B., 2018. Requirement of zebrafish pcdh10a and
815 pcdh10b in melanocyte precursor migration. Dev Biol 444 Suppl 1, S274-S286.

816 Wolff, C., Roy, S., Ingham, P.W., 2003. Multiple Muscle Cell Identities Induced by Distinct Levels
817 and Timing of Hedgehog Activity in the Zebrafish Embryo. Current Biology 13, 1169-1181.

818 Yao, S., Lum, L., Beachy, P., 2006. The ihog cell-surface proteins bind Hedgehog and mediate
819 pathway activation. Cell 125, 343-357.

820 Yin, J., Lee, R., Ono, Y., Ingham, P.W., Saunders, T.E., 2018. Spatiotemporal Coordination of FGF
821 and Shh Signaling Underlies the Specification of Myoblasts in the Zebrafish Embryo. Dev Cell 46,
822 735-750 e734.

823 Zhang, W., Hong, M., Bae, G.U., Kang, J.S., Krauss, R.S., 2011. Boc modifies the
824 holoprosencephaly spectrum of Cdo mutant mice. Dis Model Mech 4, 368-380.

825 Zhang, W., Kang, J.S., Cole, F., Yi, M.J., Krauss, R.S., 2006. Cdo functions at multiple points in the
826 Sonic Hedgehog pathway, and Cdo-deficient mice accurately model human holoprosencephaly.
827 Dev Cell 10, 657-665.

828

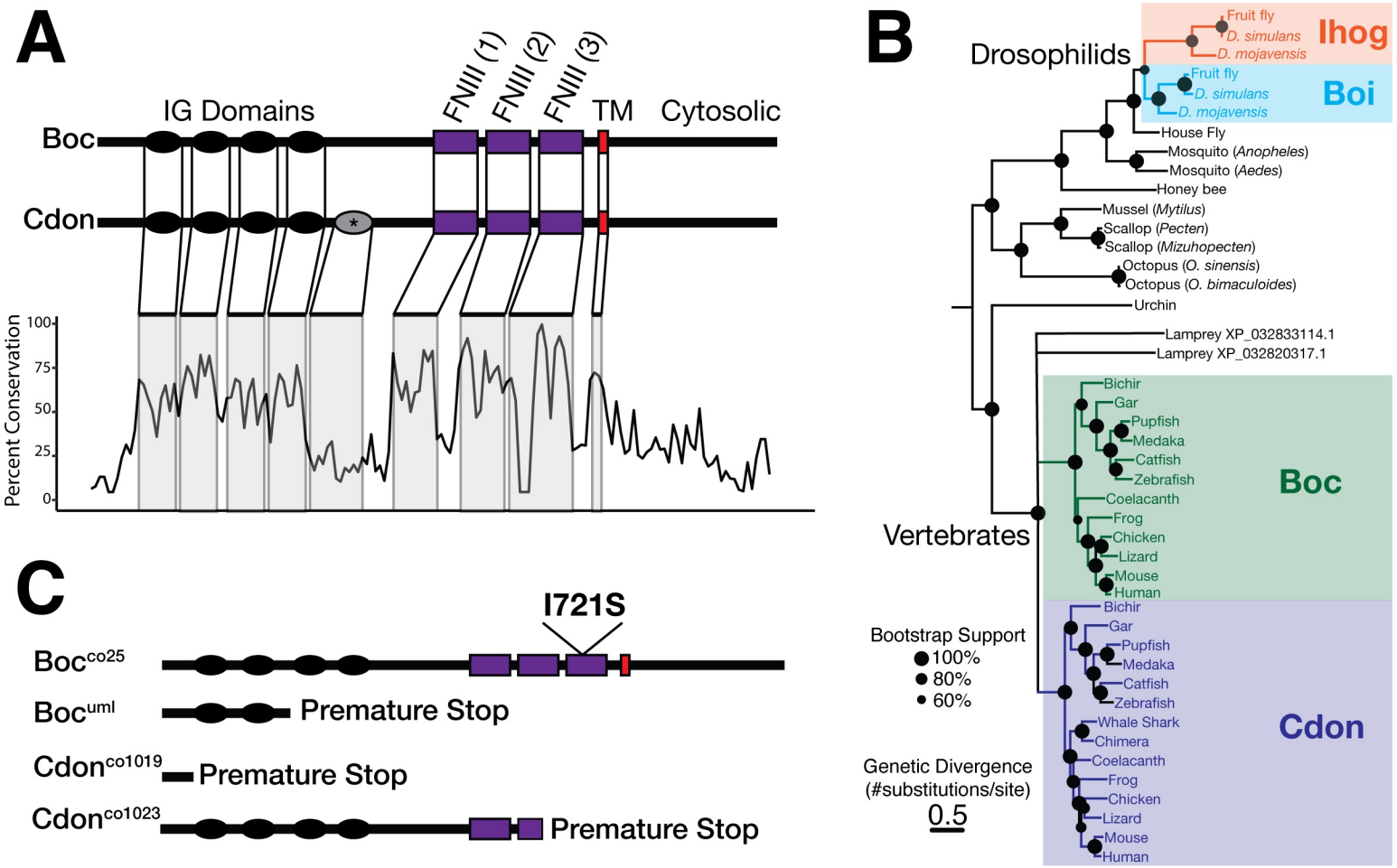
A
IG Domains
FNIII (1)
FNIII (2)
FNIII (3)
TM
Cytosolic
Boc
Cdon
*
Percent Conservation
100
75
50
25
0
B
Drosophilids
Fruit fly
D. simulans
D. mojavensis
Ihog
Fruit fly
D. simulans
D. mojavensis
Boi
House Fly
Mosquito (Anopheles)
Mosquito (Aedes)
Honey bee
Mussel (Mytilus)
Scallop (Pecten)
Scallop (Mizuhopecten)
Octopus (O. sinensis)
Octopus (O. bimaculoides)
Urchin
Lamprey XP_032833114.1
Lamprey XP_032820317.1
Bichir
Gar
Pupfish
Medaka
Catfish
Zebrafish
Coelacanth
Frog
Chicken
Lizard
Mouse
Human
Boc
Vertebrates
Bichir
Gar
Pupfish
Medaka
Catfish
Zebrafish
Whale Shark
Chimera
Coelacanth
Frog
Chicken
Lizard
Mouse
Human
Cdon
Bootstrap Support
100%
80%
60%
Genetic Divergence
(#substitutions/site)
0.5
C
I721S
Boc^co25
Boc^uml
Premature Stop
Cdon^co1019
Premature Stop
Cdon^co1023
Premature Stop

Figure 1

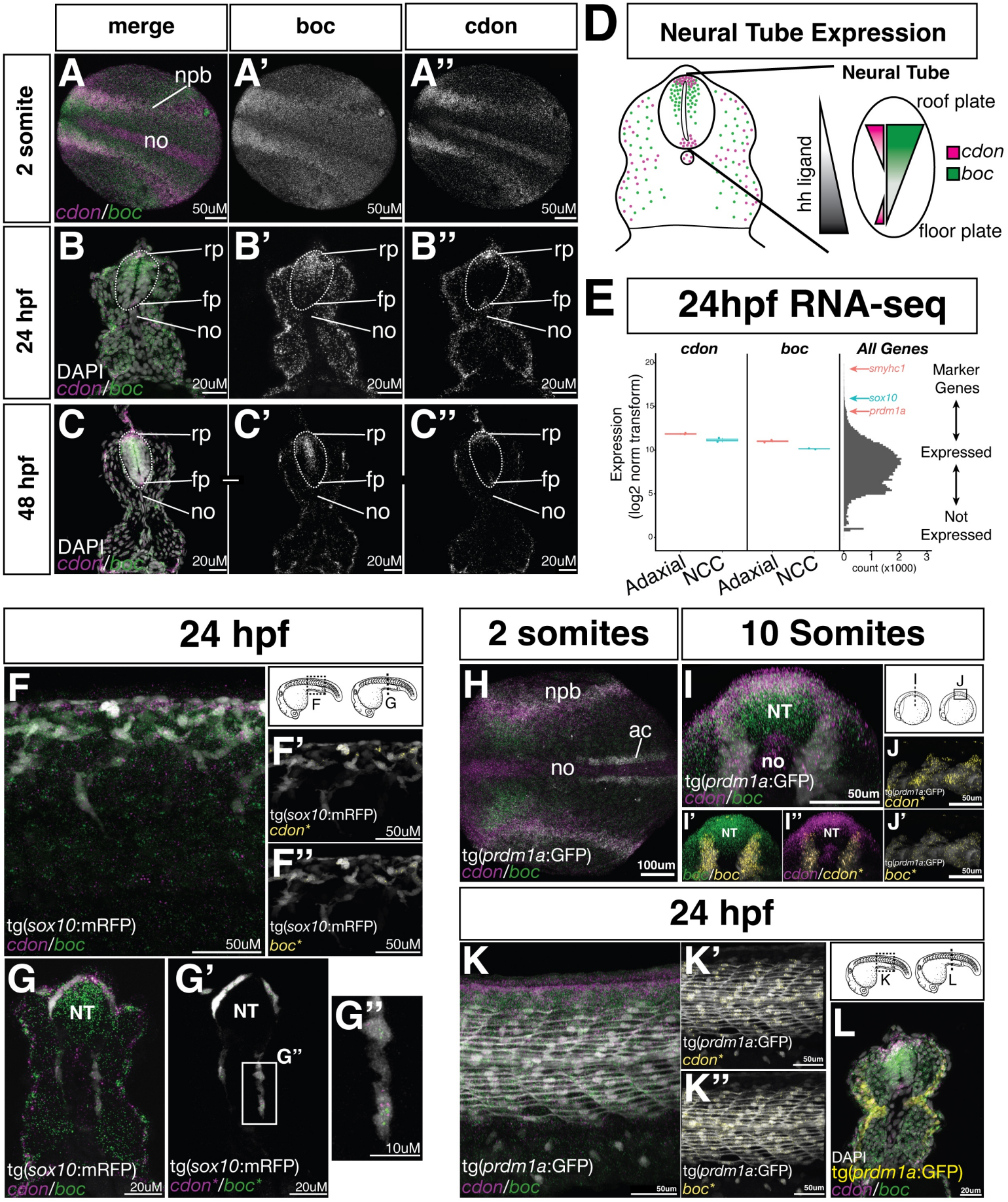
merge
boc
cdon
2 somite
24 hpf
48 hpf
A
npb
no
cdon/boc
50uM
A'
A''
B
rp
fp
no
DAPI
cdon/boc
20uM
B'
B''
C
C'
C''
D
Neural Tube Expression
Neural Tube
roof plate
hh ligand
cdon
boc
floor plate
E
24hpf RNA-seq
cdon
boc
All Genes
Expression
(log2 norm transform)
smyhc1
sox10
prdm1a
Marker
Genes
Expressed
Not
Expressed
count (x1000)
Adaxial
NCC
Adaxial
NCC
24 hpf
F
tg(sox10:mRFP)
cdon/boc
50uM
F'
tg(sox10:mRFP)
cdon*
F''
tg(sox10:mRFP)
boc*
G
NT
tg(sox10:mRFP)
cdon/boc
20uM
G'
NT
G''
tg(sox10:mRFP)
cdon*/boc*
G''
10uM
2 somites
H
npb
ac
no
tg(prdm1a:GFP)
cdon/boc
100um
10 Somites
I
NT
no
tg(prdm1a:GFP)
cdon/boc
50um
J
tg(prdm1a:GFP)
cdon*
I'
NT
boc/boc*
I''
NT
cdon/cdon*
J'
tg(prdm1a:GFP)
boc*
24 hpf
K
tg(prdm1a:GFP)
cdon/boc
K'
tg(prdm1a:GFP)
cdon*
K''
tg(prdm1a:GFP)
boc*
L
DAPI
tg(prdm1a:GFP)
cdon/boc
20um

Figure 2

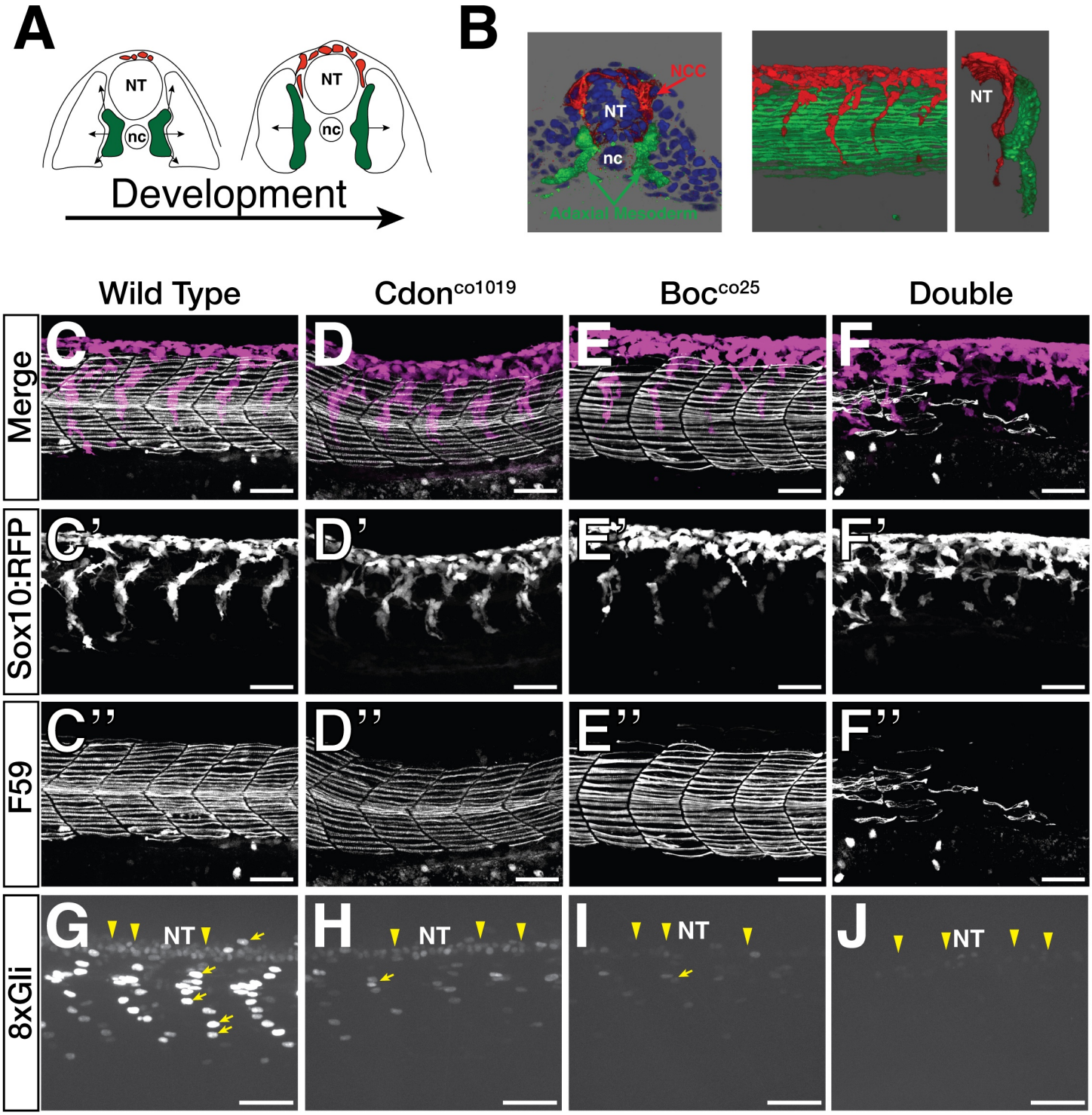
A
NT
nc
NT
nc
Development
B
NCC
NT
nc
Adaxial Mesoderm
NT
Wild Type
Cdon^{co1019}
Boc^{co25}
Double
Merge
Sox10:RFP
F59
8xGli
C
D
E
F
C'
D'
E'
F'
C''
D''
E''
F''
G
H
I
J
NT
NT
NT
NT

Figure 3

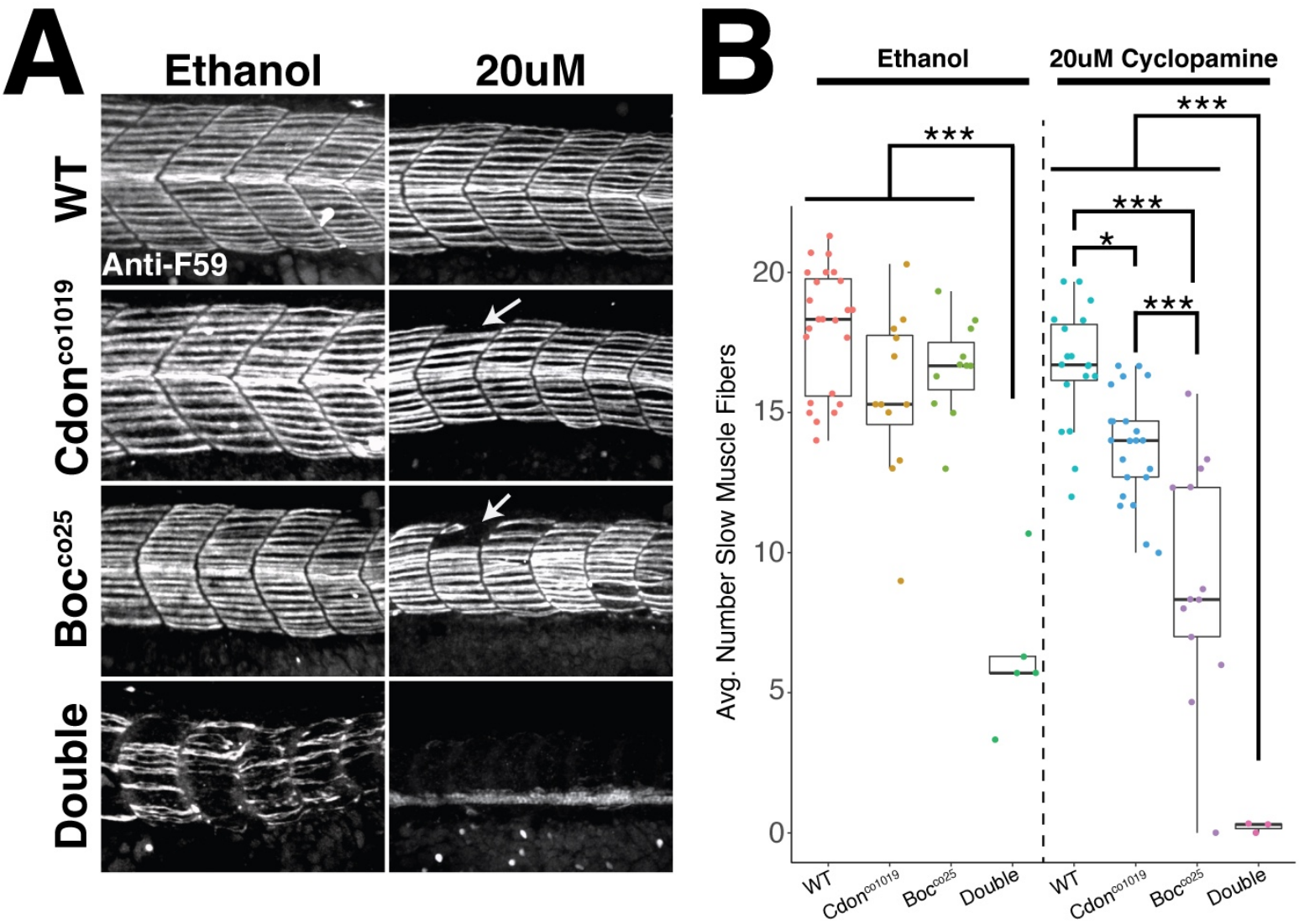
A
Ethanol
20uM
WT
Anti-F59
Cdon^co1019
Boc^co25
Double
B
Ethanol
20uM Cyclopamine
Avg. Number Slow Muscle Fibers
0
5
10
15
20
***
***
*
***
***
WT
Cdon^co1019
Boc^co25
Double
WT
Cdon^co1019
Boc^co25
Double

Figure 4

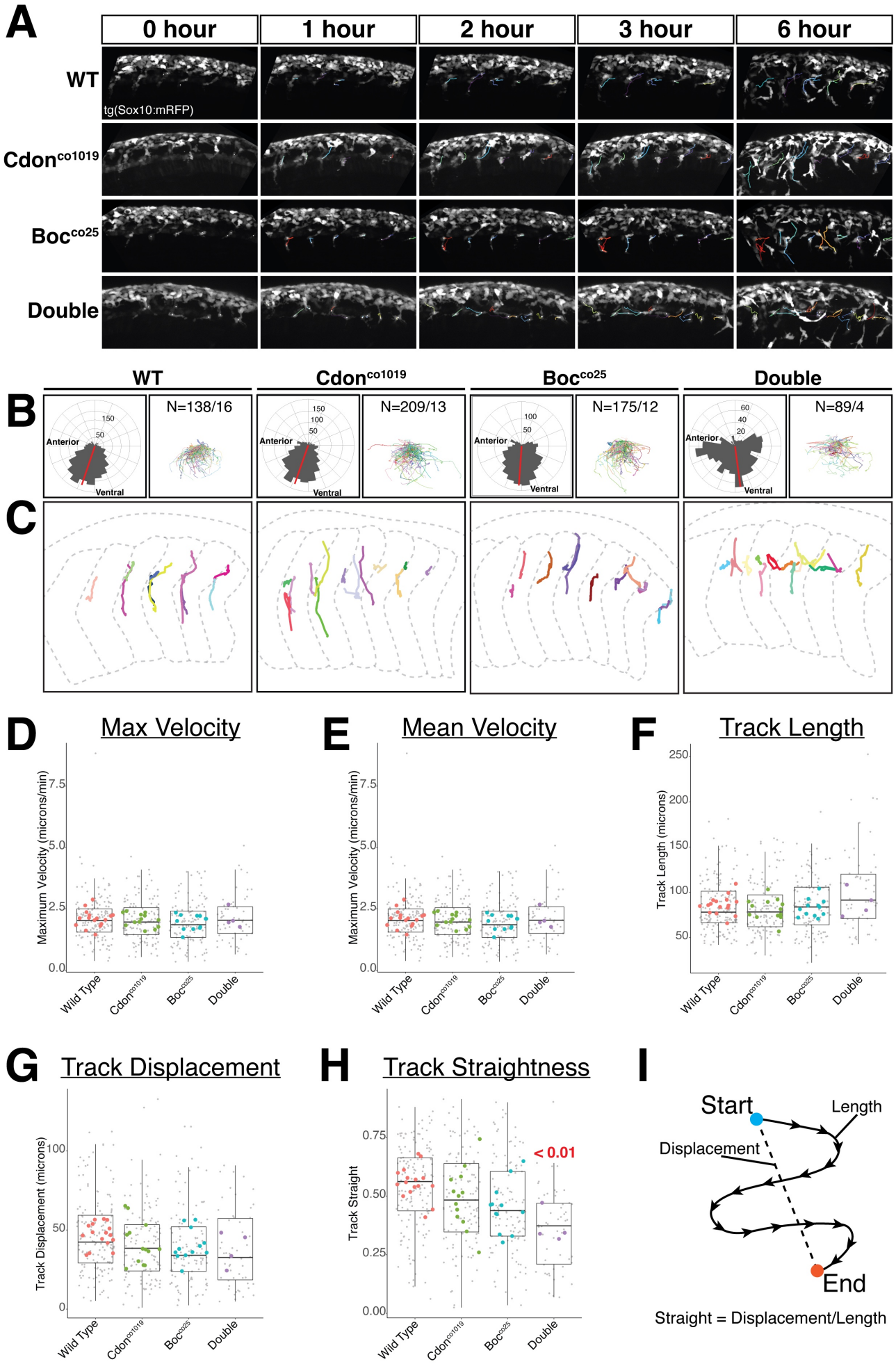
A
0 hour
1 hour
2 hour
3 hour
6 hour
WT
tg(Sox10:mRFP)
Cdon^co1019
Boc^co25
Double
B
WT
Cdon^co1019
Boc^co25
Double
N=138/16
N=209/13
N=175/12
N=89/4
Anterior
Ventral
C
D
Max Velocity
Maximum Velocity (microns/min)
E
Mean Velocity
Maximum Velocity (microns/min)
F
Track Length
Track Length (microns)
Wild Type
Cdon^co1019
Boc^co25
Double
G
Track Displacement
Track Displacement (microns)
H
Track Straightness
Track Straight
< 0.01
I
Start
Length
Displacement
End
Straight = Displacement/Length

Figure 5

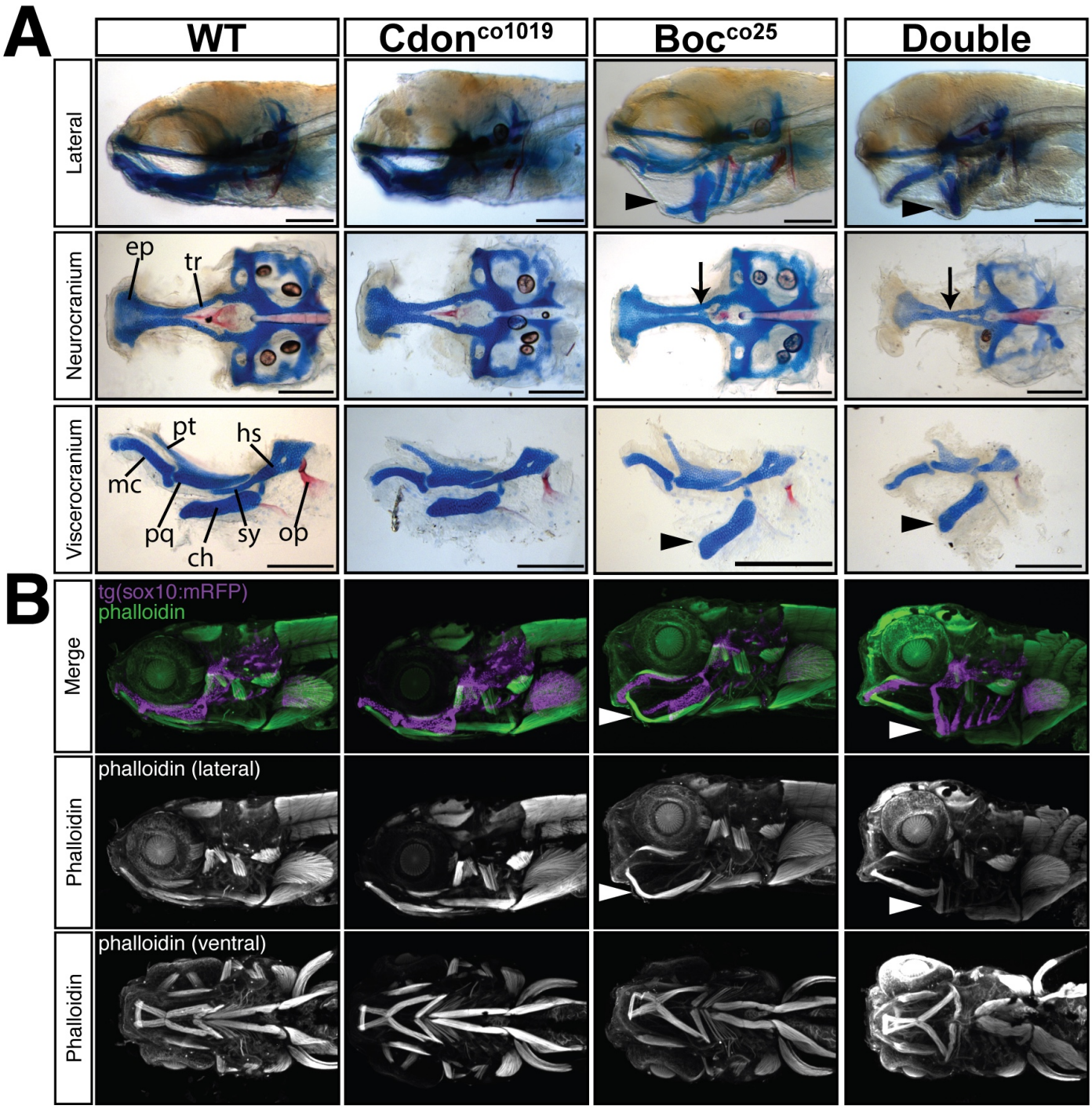
A
WT
Cdon^co1019
Boc^co25
Double
Lateral
Neurocranium
Viscerocranium
ep
tr
pt
hs
mc
pq
ch
sy
op
B
Merge
Phalloidin
Phalloidin
tg(sox10:mRFP)
phalloidin
phalloidin (lateral)
phalloidin (ventral)

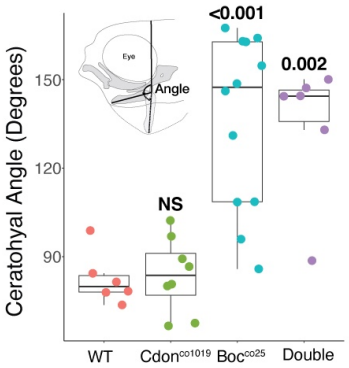
C
Ceratohyal Angle
Ceratohyal Angle (Degrees)
150
120
90
Eye
Angle
<0.001
0.002
NS
WT
Cdon^co1019
Boc^co25
Double

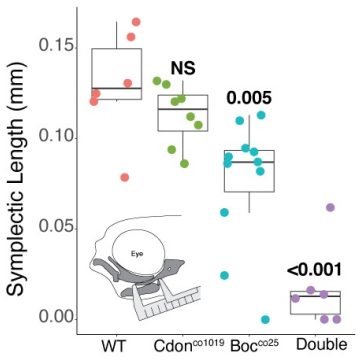
D
Symplectic Length
Symplectic Length (mm)
0.15
0.10
0.05
0.00
NS
0.005
<0.001
Eye
WT
Cdon^co1019
Boc^co25
Double

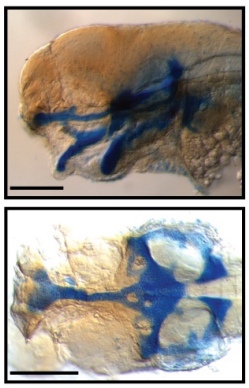
E
Cdon^co1019/co1023
Boc^co25/uml

Figure 6